ISSN 2070-0482, Mathematical Models and Computer Simulations, 2022, Vol. 14, No. 4, pp. 662–676. © Pleiades Publishing, Ltd., 2022.
Russian Text © The Author(s), 2022, published in Matematicheskoe Modelirovanie, 2022, Vol. 34, No. 1, pp. 59–80.

Determination of Thermal Properties of Gold in the Region of Melting–Crystallization Phase Transition: Molecular Dynamics Approach

V. I. Mazhukin[a], O. N. Koroleva[a, *], A. V. Shapranov[a], M. M. Demin[a], and A. A. Aleksashkina[a]

[a] *Keldysh Institute of Applied Mathematics, Russian Academy of Sciences, Moscow, Russia*

**e-mail: koroleva.on@mail.ru*

Received November 8, 2021; revised December 3, 2021; accepted December 6, 2021

Abstract—Molecular dynamics (MD) modeling of the thermophysical properties of pure metallic gold (Au) and hysteresis is considered in order to study its behavior during melting–crystallization phase transformations, i.e., in the transition from solid to liquid. The results of computational experiments are presented, in which the temperature dependences of a number of thermophysical characteristics of the metal are obtained. The possibility of the formation of highly superheated metastable states of the solid phase upon rapid heating of Au has been confirmed.

Keywords: molecular dynamics modeling, thermophysical properties, phase transitions, hysteresis

DOI: 10.1134/S2070048222040068

1. INTRODUCTION

The phenomenon of melting–crystallization of metals, which is a phase transformation of the first kind, plays an important role in materials science and engineering. In recent years, extensive experimental [1–10] and theoretical studies in combination with modeling of melting–crystallization of solids [11–21] have significantly expanded the understanding of the nature of this phenomenon. However, nonequilibrium processes of melting–crystallization, accompanied by the appearance of metastable superheated/undercooled states in the initial phase [20, 22], which are manifested in the phenomenon of thermal hysteresis [1–4, 17–21], are still of interest for research. Of particular interest is the melting mechanisms of one of the noble metals–gold, which occupies an important place among metals in terms of significance and prevalence in many branches of scientific research and innovative technological applications [23–26].

Studies of the kinetics and dynamics of phase transformations are carried out mainly by mathematical modeling methods [27]. When constructing and using continual mathematical models, it becomes necessary to take into account the dependence of material properties on temperature and pressure. For this reason, one of the most important problems of mathematical modeling is the necessity of determining thermo-physical properties in the wide temperature range (from 0.3 kK to 3–4 kK), where the decisive role is played by the phase transitions of the 1st kind (melting/crystallization, evaporation/condensation) The most important properties of the melting/crystallization processes in gold are the equilibrium melting temperature T_m, latent heat of melting L_m and the properties of heat transfer such as density $\rho(T)$, specific heat $C_p(T)$, and lattice thermal conductivity $\kappa_{lat}(T)$. The estimation of the degree of superheating/undercooling of the condensed phase during melting/crystallization is also important. It is obtained from the investigation of thermal hysteresis. Due to the limited possibilities of instrumental measurement of the thermo-physical characteristics of the material under study at high temperatures $T > T_m$, computational approaches become relevant, the main tool of which is the method of molecular dynamics (MMD). The possibilities of modeling using MMD make it possible to determine the density, enthalpy and specific heat of metals, since these characteristics are mainly determined by lattice vibrations. The contribution of the electronic subsystem to the specific heat is noticeable only at a low temperature $T < 0.01$ kK [28].

In contrast to specific heat, the contribution of the electronic component to the thermal conductivity of gold is significant. According to [29], the contribution of electronic component to the total thermal conductivity of gold is less than 95%. Since in metals the main part of heat flux is transported by conduction electrons, it was considered, that the lattice thermal conductivity does not play an essential role.

Therefore, it was not necessary to separate the total thermal conductivity into an electron and a phonon component.

Although electrons dominate the thermal and electrical transport in metals, phonons play a crucial role in the fact that electron transport is limited by electron–phonon scattering at intermediate and high temperatures (i.e., above one tenth of the Debye temperature) in the melting region [30]. In addition, electron–phonon interactions are important for superconductivity [31], the mobility of hot carriers [32], the reaction of a material upon ultrafast heating by ion bombardment or laser irradiation [33, 34], and heat transfer through metal interfaces dielectric in thermoelectric [35, 36] and plasmonic [30] devices. Separation and quantitative evaluation of the contribution of phonons to the thermal conductivity in metals is necessary for modeling electron–phonon nonequilibrium using a two-temperature model, for example, in the analysis of thermal reflection experiments, which can resolve the contributions of carrier levels to thermal conductivity [31, 37–41].

The purpose of this work is to obtain the temperature dependences of the equilibrium density, enthalpy, specific heat and phonon thermal conductivity of gold in the temperature range ($T \sim 0.3$–3.20 kK), which includes the melting region. The paper also considers the features of nonequilibrium melting and crystallization of gold based on the thermal hysteresis of enthalpy and density in the temperature range $0.60\ \text{kK} \le T \le 2.00\ \text{kK}$. The thermal hysteresis, as well as the thermophysical properties of gold, are obtained from molecular dynamics simulations. The potential of the embedded atom method (EAM) developed and tested in [42] for gold was used as the interatomic interaction potential. The article presents the results of atomistic modeling, as well as the results of comparing the obtained characteristics of gold with experimental data, showing an acceptable qualitative and quantitative agreement. Numerical and graphical information about the properties obtained and the results of comparison with experimental data are presented.

2. METHODS AND APPROACHES

The main focus of this paper is the analysis of the change in thermal physical properties at the solid–liquid phase transition and the investigation of the degree of superheating/undercooling of the condensed phase of gold on the basis of the thermal hysteresis phenomenon. The determination of the temperature dependences of thermo-physical properties of gold: density $\rho(T)$, enthalpy $H(T)$, specific heat $C_p(T)$, phonon thermal conductivity $\kappa_{lat}(T)$ in the temperature range $0.3\ \text{kK} \le T \le 3.0\ \text{kK}$, temperature and latent heat of melting at $P = 0$, as well as obtaining a thermal hysteresis of enthalpy and density is based on the atomistic approach.

For numerical solution of atomistic models, the method of molecular dynamics (MMD) is widely used. The atomistic approach is based on the model concept of multiatomic molecular system in which all atoms are represented by the material points whose motion is described by the Newton's classical equations. Atomistic models represent a system of differential equations, for integration of which the initial conditions are given as values of coordinates and velocities of all particles at the initial moment of time $t = 0$. The resulting ODE system is solved using the finite-difference Verlet scheme [43].

In MD modeling, the choice of the interaction potential between the particles plays an important role, since the reliability of the results obtained directly depends on it. To model the properties of metals, the potentials from the embedded atom method group (EAM) are mainly used. The EAM potentials take into account pair and collective interactions, the potential energy of a metal is the sum of the embedding potential of the ith atom, which depends on the effective electron density in the region where the center of the atom and the pair potential are located. In the MD modeling of the thermo-physical properties and thermal hysteresis of gold, the potential from the EAM group, developed and tested in [42] for gold, was also used, which makes it possible to describe well both the crystalline and liquid phases of the metal simultaneously.

The simulation was carried out using the widespread LAMMPS package (large-scale atomic–molecular massively parallel simulator) [44]. It implements support for many pair and many-particle short-range potentials, the ability to write atomic configurations to a text file, and also has built-in thermostats and barostats. The temperature and pressure for an ensemble of particles were controlled using the Berendsen's thermostat and barostat [45].

3. EQUILIBRIUM MELTING TEMPERATURE

The determination of the equilibrium melting temperature of gold T_m was carried out within the framework of a computational experiment based on the simultaneous existence of solid and liquid phases in the

computational domain. The calculation area was chosen in the form of a parallelepiped, with dimensions of 20 × 10 × 10 unit cells. In this case, half of the sample was presented in a solid crystalline form, and the other half in the form of a liquid. Gold has a face-centered cubic lattice with a crystal lattice constant of 0.406 nm. The total number of particles in the given region was 8000. Periodic boundary conditions were set along all three axes.

Previously, to determine the melting temperature T_m, several experiments were carried out, as a result of which an approximate value of the melting temperature $T_m \sim 1.32$ kK was obtained at a pressure $P = 0$. The entire sample was then heated to this temperature, after which one half of the sample was kept at this temperature by a thermostat, while the other half was heated to $T = 2.0$ kK. Further, in the prepared sample, the heated part is cooled by a thermostat to a temperature $T = 1.32$ kK. Then the relaxation calculation is started with the thermostat turned off at a given temperature, after which the barostat is also turned off, and the calculation continues until the phase equilibrium is established. After the onset of phase equilibrium, temperature fluctuations are observed near the equilibrium melting temperature. In this case, the temperature turned out to be $T_m = 1.332$ kK. The reference value of the equilibrium melting temperature is $T_m = 1.334$ kK [46]. Thus, the deviation of the obtained value from the reference value is 0.1%.

4. LATENT HEAT OF MELTING

The equilibrium latent heat of melting of gold L_m in this work was obtained as the difference between the enthalpies of the liquid and solid phases at the equilibrium melting temperature T_m.

The computational experiment for calculating the latent heat of melting consisted in calculating the enthalpies of the solid and liquid phases at the same temperature and pressure. For this, a cubic computational domain was prepared, which contained 13500 particles. Periodic boundary conditions were imposed in all three spatial directions of the cube. In the computational domain, an fcc crystal with a size of 15 × 15 × 15 lattice unit cells was formed from the particles. To obtain the enthalpy of the solid phase, a relaxation calculation was carried out, with the establishment of a zero average pressure using a barostat and an average temperature of 1.332 kK using a thermostat. Next, the necessary values were recorded to calculate the enthalpy of the solid phase.

To obtain the enthalpy of the liquid phase, the prepared (after relaxation) computational region at 0.30 kK was heated to 2.0 kK to obtain a liquid. This is followed by rapid cooling to a melting point of 1.332 kK. The computational region still contains liquid due to the rapid cooling. After the relaxation calculation was carried out, the necessary values were recorded to calculate the enthalpy of the liquid phase.

At the pressure $P = 0$, the value of latent heat of melting $L_m = 12.894$ kJ/mol was obtained by the conducted simulation. The known experimental value is $L_{m,\,exp} = 12.680$ kJ/mol [46]. The difference is 1.6%, which shows the possibility of using this potential for determination of the latent heat of melting.

5. CALCULATION OF DENSITY, ENTHALPY, AND SPECIFIC HEAT OF GOLD

5.1. Statement of the Problem and Computational Experiment

In this work, the temperature dependences of density $\rho(T)$, enthalpy $H(T)$, and specific heat $C_p(T)$ of gold were determined from a series of molecular dynamics calculations in a single computational experiment. We used a cubic computational region consisting of 30 × 30 × 30 elementary cells containing an fcc crystal of 108000 particles (smaller sizes cause too large fluctuations). Periodic boundary conditions were set in all directions. A premodelling relaxation procedure was performed at 0.3 kK and zero pressure. Then, the calculated region was slowly heated at a constant rate of approximately $V \approx 0.5 \times 10^9$ kK/s. Heating was continued up to a temperature of 3.5 kK, at which the sample was completely melted. The temperature dependences of density $\rho(T)$ and enthalpy $H(T)$ were recorded. The experiment was carried out at constant zero pressure $P = 0$.

5.2. Density. Modeling Results

The temperature dependence of the gold density in the temperature range $0.3\ \text{kK} \le T \le 3.5$ kK in this paper is obtained from the MD simulation. The results of the simulation after the necessary statistical processing are presented in Fig. 1. The markers in this figure show the experimental data [47, 48]. At the same equilibrium temperature ($T_m = 1.332$ kK) the density of gold melt turns out to be less than crystal density

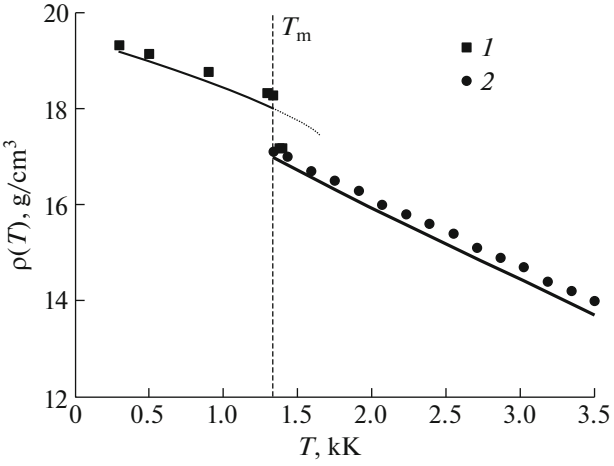

Fig. 1. Temperature dependence of density from MD calculations results; (*1*) and (*2*) are the data from the experiments [47, 48].

at the same temperature, i.e. gold, like other metals melts with reduced density which is confirmed by reference data [47]. At Fig. 1 the density reduction at overheating of the solid phase ($T > T_m$) which is $\Delta T \sim 1.24 T_m$ is clearly seen in the area of phase transition.

The value of the density difference at the solid–liquid phase transition obtained from the MD calculations corresponds well to the data of the experiment [47]. The difference from MD calculations is $\Delta\rho \approx 6\%$, according to the data of the experiment [47], it is $\Delta\rho \approx 6.4\%$. The density value at the equilibrium melting temperature differs from the reference data [47] in the solid phase by 1.4%, and in the liquid phase, by 1.1%. The density values in the liquid phase obtained from MD calculations agree well with the experimental data [48], which are slightly higher than the calculated ones. The difference is $\Delta\rho \approx 1\%$ at $T = T_m$ and $\Delta\rho \approx 2\%$ at $T = 3.5$ kK.

5.3. Enthalpy and Specific Heat. Modeling Results

The temperature dependence of the enthalpy $H(T)$ is obtained as a result of MD calculations in the range 0.3 kK $\le T \le$ 3.2 kK at constant pressure P. The results after further processing are shown in Fig. 2. For better comparison with the experimental data [49, 50], the results of MD calculations are presented by the values of enthalpy increment

$$\Delta H(T) = H(T) - H(0.298\ \text{kK}).$$

The markers in Fig. 2 show the experimental data [49, 50]. The vertical dotted line marks the melting point $T_m = 1.332$ kK obtained from MD calculations.

In the region of the phase transition of gold at the same equilibrium temperature ($T_m = 1.332$ kK), the increment in the enthalpy of the gold melt is greater than the increment in the enthalpy of crystals at the same temperature. The difference separating the solid and liquid phases in the calculations is 45.79% (Fig. 2); according to [49, 50], the enthalpy difference is 43.67 and 41.89%, respectively, which shows a fairly good agreement between the results. The dotted line in Fig. 2 shows the increase in enthalpy to $\Delta H(T) \approx 4 \times 10^4$ J/mol when the solid phase is superheated during melting. The value of superheating is $\Delta T \approx 1.24 T_m$. The energy accumulated during superheating is spent mainly on thermal vibrations of the lattice. With an increase in enthalpy in the region of the phase transition, a decrease in the density of gold occurs (Fig. 1), which indicates ongoing structural changes in the solid phase, after which melting occurs. With increasing temperature $T > T_m$, the enthalpy increment increases. At $T = 3.2$ kK, the value is $\Delta H(T) = 9.902 \times 10^4$ J/mol. The values of $\Delta H(T)$ obtained from MD calculations were compared with the data from [49, 50]. The comparison showed an almost complete agreement between the calculation results and the experimental data [50]. The maximum discrepancy with the experimental data [49], which is ≈4.7%, is observed at a temperature $T = 3.2$ kK.

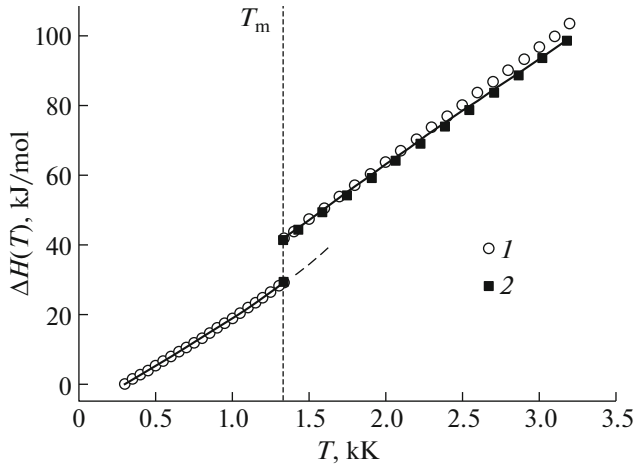

Fig. 2. Temperature dependence of the enthalpy increment $\Delta H(T)$: (*1*) is the data of the experiment [49] and (*2*) is the data of the experiment [50].

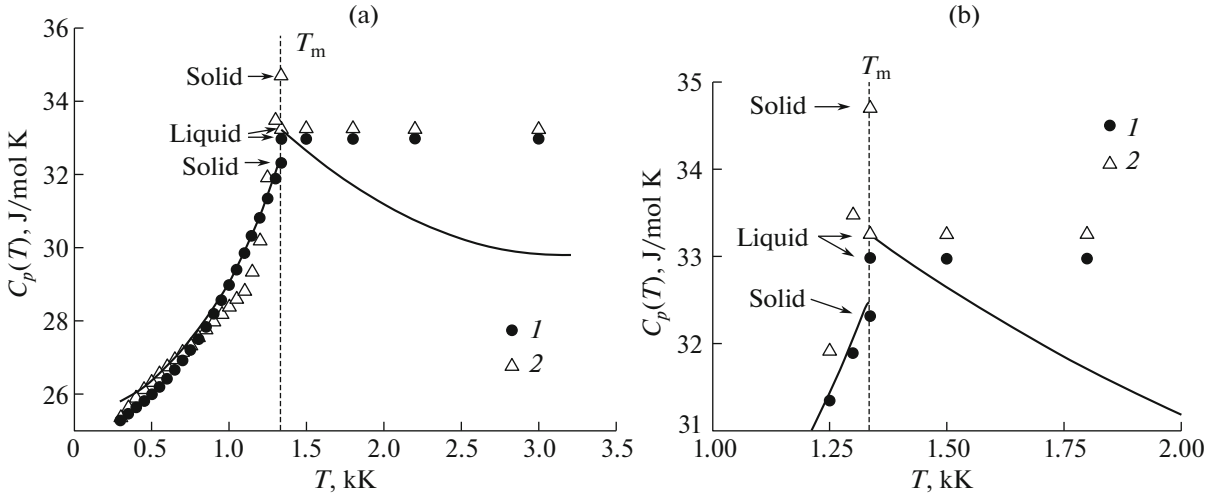

Fig. 3. (a) Temperature dependence of the specific heat of gold according to the results of MD simulation ($P = 0$): (*1*) is the data of the experiment [50] and (*2*) is the data of the experiment [51]. (b) The fragment of the phase transition region.

To calculate specific heat of gold $C_p(T)$, the values of enthalpy $H(T)$ obtained from MD calculations, were approximated separately for the solid and liquid phases by polynomials $\tilde{H}(T)$ of low degrees $m = 3$–5. The approximation error was 0.53×10^{-3} J/mol in the solid phase and 1.5×10^{-3} J/mol in the liquid phase. The temperature dependence of specific heat $C_p(T)$ in the temperature range 0.3 kK $\le T \le$ 3.2 kK at constant pressure P for each phase was determined by differentiating the corresponding dependence $\tilde{H}(T)$:

$$C_p(T) = \left(\partial \tilde{H}(T)/\partial T\right). \quad (1)$$

The calculation results are shown in Figs. 3a and 3b, and the reference and experimental results are labeled with markers [50, 51].

The vertical dotted line marks the equilibrium melting point T_m of gold. A fragment of Fig. 3a, showing with magnification the temperature dependence of the heat capacity of gold in the region of the solid–liquid phase transition, is shown in Fig. 3b.

In the solid phase, with increasing temperature, an increase in the specific heat is observed. Figures 3a and 3b show the experimental data [50, 51], with which the results of MD calculations agree very well. The maximum deviation of the results and the data from [51] is $\Delta C_p \approx 3.65\%$ at the temperature $T \approx 1.1$ kK.

Table 1. The values of the specific heat of gold at the solid–liquid phase transition

Variable	Quotation source			
	[50]	[51]	[52]	Present work
C_p, J/mol K (solid)	32.309	34.794	33.25	32.468
C_p, J/mol K (liquid)	32.970	33.24354	33.25	33.196
ΔC_p, %	2.046	−4.46	0	2.37
T_m, K	1337.33	1336	1337.33	1332

The maximum difference from the data from [50] is $\Delta C_p \approx 2.1\%$ at low temperatures $T \approx 0.30$ kK. Thus, we observe almost complete agreement. Figure 3b clearly shows that at the same equilibrium temperature ($T_m = 1.332$ kK), specific heat of gold melt is greater than specific heat of crystals at the same temperature. The increase in specific heat is small and amounts to ~2.37%. The few experimental data on the existence of a difference in the value of the heat capacity of gold at the phase transition and its magnitude have a spread (Table 1). The values of the equilibrium melting temperature T_m also have a spread.

The specific heat of gold decreases as the temperature rises and for $T > 2.027T_m$ the magnitude of specific heat is almost constant in liquid and amounts to $C_p(T) \approx 29.8$ J/mol K. This behavior of the specific heat in the liquid phase shows good agreement with the results of [52].

6. PHONON THERMAL CONDUCTIVITY

6.1. Statement of the Problem and Computational Experiment

The phonon thermal conductivity coefficient κ_{lat} of gold was determined from the phenomenological Fourier relation for the heat flux W [53]:

$$W = -\kappa_{lat}\partial T/\partial x, \tag{2}$$

where W is the heat flux, T is the temperature, and x is the coordinate in the direction of the flux.

MD modeling based on the direct nonequilibrium method [54, 55] was used to calculate the phonon thermal conductivity coefficient κ_{lat}. The direct non-equilibrium method consists of creating heat source and heat sink regions in the simulation cell to superimpose a constant heat flow along the direction of interest. Therefore, the computational algorithm is built according to a scheme close to the scheme of experimental measurements of the coefficient κ_{lat}.

The calculation of the phonon thermal conductivity of gold was carried out within the framework of the following computational experiment. We considered a region in the form of a parallelepiped with dimensions of 10 × 10 × 40 elementary cells, corresponding to 16000 particles, with periodic boundary conditions in all three directions. The interatomic interaction potential EAM was used as the interaction potential [42].

The area along the x axis was divided into the number of intervals corresponding to the number of elementary cells along this axis, which, in turn, corresponds to the number of particles. Heating was carried out in the first interval of the computational domain, the sink interval was located in the middle of the domain. At each time step, a constant amount of heat δQ_N was added to the heating region and the same amount was taken from the sink region. The heat flux W was calculated as

$$W = dQ/(SNdt)/2, \tag{3}$$

where $dQ = N \times dt \times \delta Q_N$ is the total added energy, where δQ_N is the energy added during 1 time step, N is the number of steps, dt is the size of time step, and S is the area cross section. The time step dt was chosen for low temperatures 0.30 kK ≤ T ≤ 1.0 kK to be equal to 3 fs, for 1.0 kK < T ≤ T_m equal to 2 fs, and for high temperatures $T > T_m$ equal to 1 fs. Division by 2 is used because of periodic boundary conditions, i.e., heat spreads in two directions. The resulting temperature gradient was then calculated and Fourier's law (2) was used to obtain the thermal conductivity. The procedure for calculating the thermal conductivity is detailed in [56, 57].

To improve the accuracy of calculations, the temperature difference was calculated not over the entire interval between the source and sink, but over its central part with a length of 0.8 of the total length. This range was chosen due to the fact that when approaching heat sources and sinks, the temperature profile

Table 2. The error of calculation of the thermal conductivity coefficient

T, kK	0.30	0.60	0.90	1.332 (solid phase)	1.332 (liquid phase)	0.20
δ, %	0.2	1.2	0.8	2.3	3.2	2.6

has a highly nonlinear character. For calculations according to the Fourier law, it is important to obtain a stationary spatial temperature profile, which is equivalent to obtaining a constant heat flux. For this, the following condition must be met: the size of the simulation cell must be significantly larger than the mean free path of phonons. This leads to the consideration of large samples, several million atoms, which goes beyond the scope of nanoscale regions. This size of the computational domain, in turn, leads to too much computational resources. For such cases, it becomes necessary to calculate the thermal conductivity for several different sample sizes and then perform the scaling procedure [58–60]. To overcome the effects of a finite size, the heat flux was determined from the results of a series of calculations. Calculations were carried out for different lengths of the computational region L_n: 40, 80, 160, 240, and 320 single cells with a constant cross section $S = 10 \times 10$ cells at the same temperature.

Next, the scaling procedure was carried out, which is as follows: for each temperature value, the inverse dependence of the thermal conductivity $1/\kappa_{lat}$ was plotted versus the reciprocal of the length L_n of the computational domain ($1/L_n$), and the thermal conductivity was determined by extrapolating the data $1/L_n \to 0$ [59]. This procedure is justified by the expression for thermal conductivity obtained from the kinetic theory [54, 55]. The procedure was repeated for all required temperatures in the range 0.30 kK $\le T \le$ 2.0 kK. Table 2 presents the error values δ for calculating the values of the thermal conductivity coefficient for various temperatures.

As we can see, the calculation error is $\delta \le 3.2\%$. Such an error is acceptable for further use of the phonon thermal conductivity coefficient $\kappa_{lat}(T)$ in two-temperature mathematical models.

6.2. Modeling Results

Figure 4 shows the temperature dependence of the phonon thermal conductivity of gold, obtained as a result of calculations. At the temperature 0.30 kK, the value of phonon thermal conductivity is κ_{lat} = 3.41 W/mK. As the temperature increases, the thermal conductivity of gold decreases. The region of the solid–liquid phase transition, is shown in an magnified view in a fragment of Fig. 4. At the equilibrium temperature T_m = 1.332 kK, the value of thermal conductivity in the solid phase is κ_{lat} = 0.6 W/mK, and in the liquid phase at the same temperature, κ_{lat} = 0.49 W/mK. At the equilibrium melting temperature T_m = 1.332 kK, the difference in thermal conductivity at the solid–liquid phase transition is 18%. The calculation was carried out up to a temperature T = 2.0 kK, at which the value of thermal conductivity is κ_{lat} = 0.48 W/mK. Such a change in the phonon thermal conductivity with increasing temperature does not contradict the ideas about the behavior of the phonon thermal conductivity of metals.

Comparison with alternative calculations [29, 61, 62] showed good agreement. At low temperatures (0.30 kK $\le T <$ 0.60 kK) the highest deviation from [29, 62] is $\Delta\kappa_{lat} \sim 32\%$. As the temperature rises, the difference of the results becomes less.

At T = 0.60 kK [62] the difference is $\Delta\kappa_{lat} \sim 12\%$, and at T = 0.90 kK the results are almost exactly the same $\Delta\kappa_{lat} \sim 2\%$. The agreement with the results of [61] is less. In the temperature range $T >$ 1.0 kK, there are no data to compare.

It is of interest to estimate the contribution of phonon thermal conductivity to the total thermal conductivity $\kappa = \kappa_{lat} + \kappa_e$ (κ_e is the electron thermal conductivity). According to the estimates from [29] at 0.30 kK, the ratio of the phonon thermal conductivity to total one for various metals can be less than 2% or reach 40% [29]. Using the values of the total thermal conductivity of gold [46] at temperatures $T \le$ 1.0 kK, the contribution of the phonon thermal conductivity to the total one κ_{lat}/κ was calculated. The results are shown in Fig. 5.

At T = 0.3 kK the contribution of the phonon thermal conductivity of gold κ_{lat} to the total one κ is 1.08%. As the temperature rises, the contribution of the phonon thermal conductivity decreases to 0.3% at T = 1.0 kK. Despite such a small contribution to the total thermal conductivity, the phonon thermal conductivity plays an important role in the heat transfer of gold, especially for metallic nanostructures due to a significant decrease in κ_e in the nanostructure [63]. Thus, the results of our calculations show the need to study the heat transfer of phonons in metals.

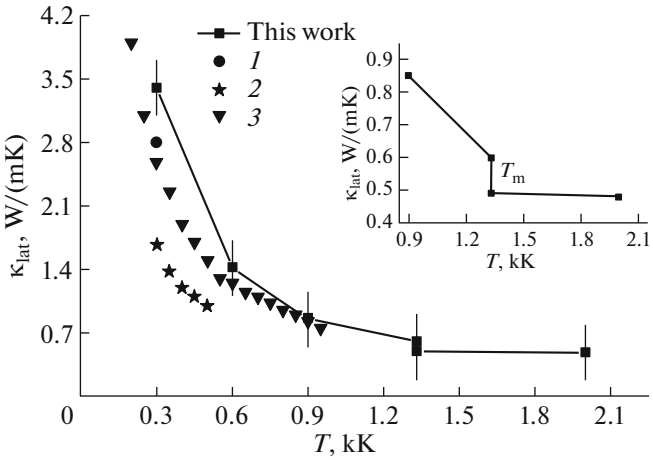

Fig. 4. Temperature dependence of the phonon thermal conductivity of gold. The markers (*1*–*3*) show the calculation results from [29, 61, 62], respectively.

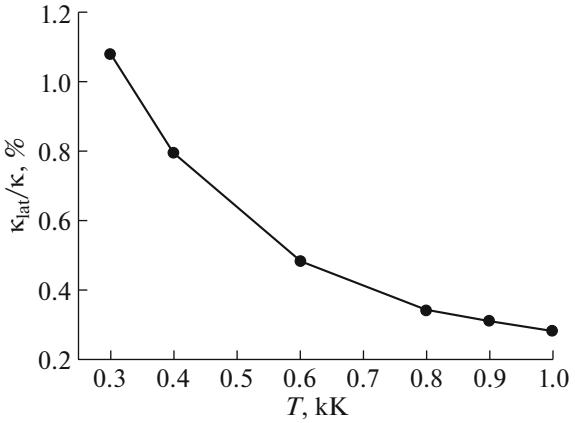

Fig. 5. Temperature dependence of the contribution of the phonon thermal conductivity of gold to the total thermal conductivity.

In general, such comparison results give grounds to believe that the chosen method and potential describe the model with good accuracy and are applicable for further research.

7. INVESTIGATION OF THE DEGREE OF SUPERHEATING/UNDERCOOLING IN THE REGION OF THE PHASE TRANSITION

The nonequilibrium behavior of melting–crystallization processes manifests itself in the phenomenon of thermal (heat) hysteresis. The study of thermal hysteresis was carried out by many researchers both experimentally [1–4] and theoretically [17–21]. The studies were carried out mainly with the aim of analyzing the size effect and the influence of the interfacial structure on the melting processes [2, 4, 5, 7, 17, 21], studying the degree of superheating–undercooling of metals [1–3, 18–20] and the influence of thermal hysteresis on the properties of metals [2, 17, 18].

Thermal hysteresis is characterized by a mismatch between the melting and crystallization temperatures $T_{sl} \neq T_{cr}$, as well as the thermodynamic characteristics of the material (enthalpy, density) during heating and cooling. The value of thermal hysteresis is a characteristic of the degree of superheating-undercooling of the condensed phase; therefore, it is of particular interest for studying nonequilibrium melting–crystallization. The experimental approach to studying the thermal hysteresis of materials, which is traditional, has a number of limitations in terms of the range of measurement conditions, especially in the melting region. It is known that experiments on the study of undercooling of metals [10] are well

described in the literature, in contrast to studies of superheating. Because of this, it is important to use the theoretical approach [11–17, 19–21, 42, 64].

7.1. Statement of the Problem and Computational Experiment

In the present work, the determination of the thermal hysteresis of the enthalpy and density for gold is based on the atomistic approach. The simulation was carried out in the temperature range 0.60 kK ≤ T ≤ 2.00 kK using the widespread LAMMPS package [44]. The temperature and pressure for the ensemble of particles were controlled using the Berendsen's thermostat and barostat [45].

In our work, from a series of molecular dynamics calculations within the framework of one computational experiment, the enthalpy and density of gold were determined in the isobaric process of heating and cooling, including phase transitions. For the computational experiment, a calculation area was chosen in the form of a cube, with dimensions of 30 × 30 × 30 elementary cells, containing an fcc crystal of 108000 particles. Periodic boundary conditions were set in all directions. The particle velocities were set in accordance with the Maxwell distribution at a temperature of 0.60 kK. The relaxation procedure preceding the simulation was carried out at a temperature of 0.30 kK and zero pressure. Next, the sample was heated at a constant rate approximately equal to $V \sim 0.56 \times 10^9$ kK/s. Heating continued up to a temperature of 2.0 kK, at which the sample was completely melted, which made it possible to record the temperature dependences of the density $\rho(T)$ and enthalpy $H(T)$ during heating. At the same time, the sample was prepared for cooling and subsequent recording of the dependences of density $\rho(T)$ and enthalpy $H(T)$ during cooling. Cooling of the sample, as well as its heating, was carried out at the same constant rate V. The experiments were carried out at a constant zero pressure $P = 0$.

7.2. Modeling Results

The results of MD simulation of the enthalpy and density hysteresis are shown in Figs. 6 and 7. Figure 6 shows the thermal enthalpy hysteresis loop, which is represented by the generally accepted values of the increment $\Delta H(T) = H(T) - H(0.298\ \text{kK})$. The hysteresis of gold density is shown in Fig. 7. The vertical dotted lines in the figures mark the equilibrium melting temperature T_m, the end temperature of melting T_{sl}, the end temperature of crystallization T_{cr}, the limiting temperatures of overheating of the solid phase T^+, and undercooling of the liquid phase T^- which are the temperatures of the beginning of melting and the beginning of crystallization, respectively. These temperatures determine the vertices of the hysteresis contour, which is denoted by the letters *ABCDEF* in Figs. 6 and 7.

The thermal hysteresis loop (Figs. 6 and 7) is formed when the heating (solid line) and cooling (dashed line) curves are combined, taking into account the direct (melting) and reverse (crystallization) phase transitions. The directions of the heating and cooling processes are shown in Figs. 6 and 7 by arrows.

The heating of the solid phase of gold occurs with the absorption of thermal energy (endoprocess) and is accompanied by its overheating, $T > T_m$, and the formation of a metastable state. As the crystal heats up,

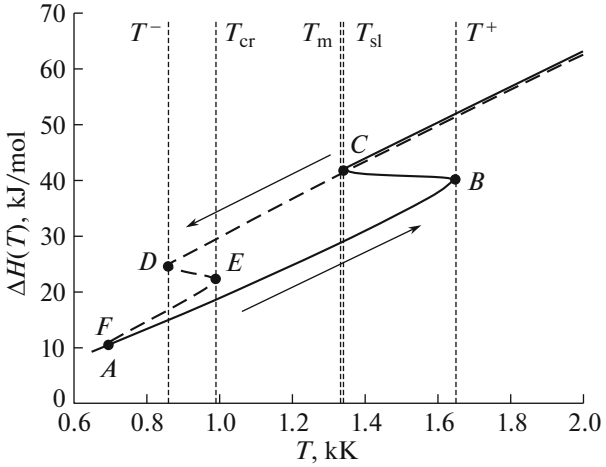

Fig. 6. Thermal hysteresis of the enthalpy of gold.

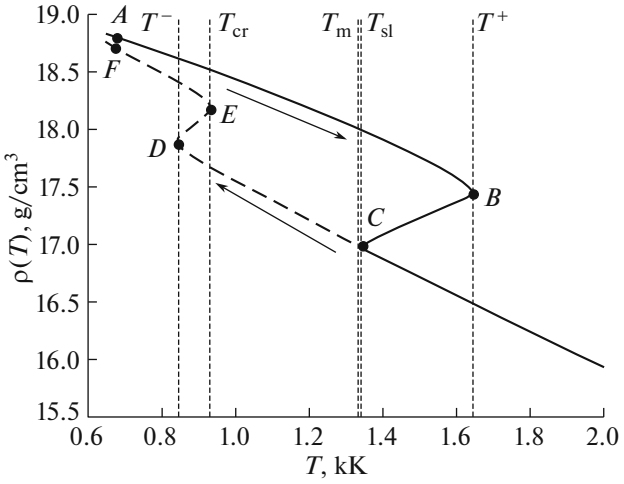

Fig. 7. Thermal hysteresis of the density of gold.

its thermal expansion occurs. The formation of a metastable state is accompanied by a further drop in the density of the solid phase (Fig. 7). The limiting superheating of the metastable state is reached at point B of the hysteresis contour (Figs. 6 and 7) at a temperature $T^+ \approx 1.235T_m$, which is the temperature at which melting begins. At point B, the first stable nuclei of a new liquid phase are formed. On segment BC of the hysteresis contour, the nuclei begin to grow rapidly due to the fact that their boundaries, representing melting fronts, quickly run over the superheated solid phase, absorbing the energy L_m.

In this case, the melting fronts always turn out to be superheated with respect to the temperature T_m. At point C, the solid phase completely disappears. In our calculation, due to the low heating rate $V \sim 0.56 \times 10^9$ kK/s, the melting end temperature is higher than the equilibrium melting temperature T_m, $T_{sl} - T_m = 8$ K. At a higher heating rate, the difference between these temperatures can be significant [33, 65]. With further heating, thermal expansion of the liquid occurs.

From MD modeling results, relative superheating of the solid phase, which is observed in the enthalpy (Fig. 6) and density (Fig. 7) hysteresis, is $\theta^+ = (T^+ - T_m)/T_m \approx 0.235$. For the heating rate $V = 10^9$ kK/s, the relative superheating of gold is obtained in [20] from MD calculations (lower index md) $\theta^+_{md} \approx 0.3$ and from the calculation using classic theory of homogeneous nucleation (lower index ns is the nucleation in the solid phase) $\theta^+_{ns} \approx 0.2$. Relative superheating of solid phase of gold was also obtained in [66], which amounted to $\theta^+_{ns} \approx 0.184$. From comparison, the obtained results are in good agreement with the results of [20, 66]. According to estimations from [17, 20], metals can be superheated to the temperature of the initiation of massively homogeneous transformation $T^+ \approx 1.3T_m$, which is also in agreement with the results for gold in the present paper.

Target cooling, in contrast to heating, occurs with heat release and is an exoprocess. Crystallization turns out to be much more demanding on the cooling rate. The limiting temperature of undercooling of the liquid phase of gold (point D on the hysteresis contour, Figs. 6 and 7), which is $T^- \approx 0.646T_m$, is the temperature of the beginning of crystallization, at which the formation of the first stable nuclei of a new solid phase occurs. On the segment DE of the hysteresis contour (Figs. 6 and 7), there is a rapid growth of the formed nuclei of a new phase due to the rapid movement of their boundaries along the undercooled liquid phase, representing the fronts of crystallization. In this case, the crystallization fronts are always undercooled with respect to the equilibrium melting temperature T_m. At the point E (temperature $T_{cr} = 0.983$ kK), liquid phase completely disappears. In our calculation due to the high cooling rate $V \sim 0.56 \times 10^9$ kK/s, the ending temperature of crystallization T_{cr} is lower than the equilibrium melting temperature T_m, $T_m - T_{cr} = 0.342$ kK. The too high cooling rate in our calculation led to the fact that the density of the substance at the temperature T_{cr} turned out to be less than the density of the crystal by 1.7%. The density of the new phase, despite a constant increase, remains less than the crystalline one (straight line EF of the hysteresis contour in Fig. 7).

Relative undercooling of the liquid phase, which is observed in the enthalpy (Fig. 6) and density (Fig. 7) hysteresis, from the results of MD modeling was $\theta^- = (T_m - T^-)/T_m \approx 0.354$. A comparison with the results of [20], obtained from MD calculations and from a calculation using the classic theory of homogeneous nucleation respectively, $\theta^-_{md} \approx 0.44$, $\theta^-_{ns} \approx 0.25$, shows a good agreement.

The maximum value of hysteresis in this work was $\Delta T_{hyst} = T^+ - T^- \approx 0.589 T_m$, which is consistent with the estimate of the hysteresis width for metals, which is $0.66 T_m$ [17].

The resulting hysteresis of the enthalpy and density of gold demonstrates the formation of metastable regions and the non-equilibrium nature of the processes of gold melting–crystallization.

8. CONCLUSIONS

Molecular dynamics modeling of the thermophysical properties of gold, hysteresis, equilibrium melting temperature of gold $T_m = 1.332$ kK and specific heat of melting $L_m = 1.289 \times 10^4$ J/mol at $P = 0$ has been performed. In the framework of one computational experiment in the range 0.3 kK $\le T \le$ 3.2 kK, temperature dependences of such thermo-physical characteristics of gold as enthalpy, specific heat $C_p(T)$, density $\rho(T)$ were obtained with the transition through the melting point. In the region of the melting–crystallization phase transition, all the obtained thermo-physical properties of gold at the equilibrium melting temperature T_m have different values in the solid and liquid phases. This corresponds to the characteristics of first-order phase transitions. A comparison with the results of alternative calculations and experimental results [47–52] showed a good agreement.

The phonon thermal conductivity $\kappa_{lat}(T)$ of gold is obtained. At the equilibrium melting temperature $T_m = 1.332$ kK, the difference in thermal conductivity at the solid–liquid phase transition is 18%. The change in the phonon thermal conductivity with increasing temperature does not contradict the ideas about the behavior of the phonon thermal conductivity of metals. Comparison with alternative calculations [29, 61, 62] shows a good agreement. The contribution of phonon thermal conductivity to the total thermal conductivity, which in the solid phase varies from 0.3% (at 1.0 kK) to 1.08% (at 0.3 kK), is estimated, which corresponds to the estimates from [29]. Although electrons dominate thermal and electrical transport in metals, phonons play a decisive role in that electron transport is limited by electron–phonon scattering at intermediate and high temperatures in the melting region [30]. The phonon thermal conductivity plays an important role in the heat transfer of gold, especially for metallic nanostructures due to a significant decrease in κ_e in the nanostructure [63]. Thus, the results of our calculations show the need to study the heat transfer of phonons in metals.

From a series of molecular dynamics calculations in the framework of one computational experiment, the hysteresis of the enthalpy and density of gold was obtained in the range 0.6 kK $\le T \le$ 2.0 kK. The resulting hysteresis of the enthalpy and density of gold demonstrates the formation of metastable regions and the nonequilibrium nature of the processes of melting–crystallization of gold. An analysis of the thermal hysteresis at a heating and cooling rate of $V \sim 0.56 \times 10^9$ kK/s made it possible to estimate the degree of superheating–undercooling of the condensed phase. The obtained limiting superheating temperature of the metastable state of the solid phase and relative superheating, as well as the limiting undercooling temperature and relative undercooling of the liquid phase of gold are in good agreement with the results of alternative calculations [17, 20, 66]. The maximum value of hysteresis, which is $\Delta T_{hyst} \approx 0.589 T_m$, agrees with the estimate of the hysteresis width for metals, which is $0.66 T_m$ [17].

FUNDING

The work was supported by Russian Science Foundation, project no. 18-11-00318.

CONFLICT OF INTEREST

The authors declare that they have no conflicts of interest.

REFERENCES

1. Q. Xu, I. D. Sharp, C. W. Yuan, D. O. Yi, C. Y. Liao, A. M. Glaeser, A. M. Minor, J. W. Beeman, M. C. Ridgway, P. Kluth, J. W. Ager, D. C. Chrzan, and E. E. Haller, "Large melting-point hysteresis of Ge nanocrystals embedded in SiO_2," Phys. Rev. Lett. **97** (15), 155701 (2006). https://doi.org/10.1103/PhysRevLett.97.155701

2. H. K. Christenson, "Confinement effects on freezing and melting," J. Phys.: Condens. Matter **13** (11), R95–R133 (2001).
https://doi.org/10.1088/0953-8984/13/11/201
3. A. L. Pirozerski, O. I. Smirnova, A. I. Nedbai, O. L. Pirozerskaya, N. A. Grunina, and V. M. Mikushev, "Peculiarities of melting and crystallization of n-decane in a porous glass," Phys. Lett. A **383** (30), 125872 (2019).
https://doi.org/10.1016/j.physleta.2019.125872
4. K. K. Nanda, "Bulk cohesive energy and surface tension from the size-dependent evaporation study of nanoparticles," Appl. Phys. Lett. **87** (2), 021909 (2005).
https://doi.org/10.1063/ 1.1994958
5. V. D. Aleksandrov and V. A. Postnikov, "The effect of sample mass on the crystallization supercooling in bismuth melt," Tech. Phys. Lett. **29** (4), 287–289 (2003).
https://doi.org/10.1134/ 1.1573293
6. T. T. Järvi, A. Kuronen, K. Meinander, K. Nordlund, and K. Albe, "Contact epitaxy by deposition of Cu, Ag, Au, Pt, and Ni nanoclusters on (100) surfaces: Size limits and mechanisms," Phys. Rev. B **75** (11), 115422 (2007).
https://doi.org/10.1103/PhysRevB.75.115422
7. J-P. Borel, "Termodynamic size effect and the structure of metallic clusters," Surf. Sci. **106**, 1–9 (1981).
8. D. R. Uhlmann, "On the internal nucleation of melting," J. Non-Cryst. Solids **41** (3), 347–357 (1980).
https://doi.org/10.1016/0022-3093(80)90180-5
9. R. Kofman, P. Cheyssac, A. Aouaj, Y. Lereah, G. Deutscher, T. Ben-David, J. M. Penisson, and A. Bourret, "Surface melting enhanced by curvature effects," Surf. Sci. **303** (1–2), 231–246 (1994).
https://doi.org/10.1016/0039-6028(94)90635-1
10. K. F. Kelton, "Crystal nucleation in liquids and glasses," Solid State Phys. **45**, 75–177 (1991).
https://doi.org/10.1016/S0081-1947(08)60144-7
11. V. I. Mazhukin, A. V. Shapranov, M. M. Demin, and N. A. Kozlovskaya, "Temperature dependence of the kinetics rate of the melting and crystallization of aluminum," Bull. Lebedev Phys. Inst. **43** (9), 283–286 (2016).
https://doi.org/10.3103/S1068335616090050
12. V. I. Mazhukin, A. V. Shapranov, V. E. Perezhigin, O. N. Koroleva, and A. V. Mazhukin, "Kinetic melting and crystallization stages of strongly superheated and supercooled metals," Math. Models Comput. Simul. **9** (4), 448–456 (2017).
https://doi.org/10.1134/S2070048217040081
13. L. Wu, Y. Zhu, H. Wang, and M. Li, "Crystal–melt coexistence in fcc and bcc metals: a molecular-dynamics study of kinetic coefficients," Modell. Simul. Mater. Sci. Eng. **29** (6), 065016 (2021).
https://doi.org/10.1088/1361-651X/ac13c9
14. V. I. Mazhukin, A. V. Shapranov, A. V. Mazhukin, and O. N. Koroleva, "Mathematical formulation of a kinetic version of Stefan problem for heterogeneous melting/crystallization of metals," Math. Montis. **36**, 58–77 (2016).
15. Z.-L. Liu, J.-S. Sun, R. Li, X.-L. Zhang, and L.-C. Cai, "Comparative study on two melting simulation methods: melting curve of gold," Commun. Theor. Phys. **65** (5), 613–616 (2016).
https://doi.org/10.1088/0253-6102/65/5/613
16. B. Rethfeld, K. Sokolowski-Tinten, D. von der Linde, and S. I. Anisimov, "Ultrafast thermal melting of laser-excited solids by homogeneous nucleation," Phys. Rev. B **65** (9), 092103 (2002).
https://doi.org/10.1103/PhysRevB.65.092103
17. L. A. Borynyak and A. P. Chernyshev, "A temperature hysteresis at melting and crystallization of nanoobjects," Nauchn. Vestn. Novosib. Gos. Tekhn. Univ., No. 1 (54), 172–179 (2014).
18. V. D. Aleksandrov, O. A. Pokyntelytsia, and A. Yu. Sobolev, "Thermal hysteresis during the melting and crystallization of macroobjects," Tech. Phys. **62** (5), 741–744 (2017).
https://doi.org/10.1134/S1063784217050036
19. L. J. Lewis, P. Jensen, and J.-L. Barrat, "Melting, freezing, and coalescence of gold nanoclusters," Phys. Rev. B **56** (4), 2248–2257 (1997).
https://doi.org/10.1103/PhysRevB.56.2248
20. S.-N. Luo, T. J. Ahrens, T. Çağın, A. Strachan, W. A. Goddard, and D. C. Swift, "Maximum superheating and undercooling: Systematics, molecular dynamics simulations, and dynamic experiments," Phys. Rev. B **68** (13), 134206 (2003).
https://doi.org/10.1103/ PhysRevB.68.134206
21. Q. S. Mei and K. Lu, "Melting and superheating of crystalline solids: From bulk to nanocrystals," Prog. Mater. Sci. **52** (8), 1175–1262 (2007).
https://doi.org/10.1016/j.pmatsci.2007.01.001
22. S. Williamson, G. Mourou, and J. C. M. Li, "Time-resolved laser-induced phase transformation in aluminum," Phys. Rev. Let. **52** (26), 2364–2367 (1984).
https://doi.org/10.1103/ PhysRevLett.52.2364

23. S. Jendrzej, B. Gökce, M. Epple, and S. Barcikowski, "How size determines the value of gold: Economic aspects of wet chemical and laser-based metal colloid synthesis," Chem. Phys. Chem. **18** (9), 1012–1019 (2017). https://doi.org/10.1002/cphc.201601139
24. N. Elahi, M. Kamali, and M. H. Baghersad, "Recent biomedical applications of gold nanoparticles: A review," Talanta **184**, 537–556 (2018). https://doi.org/10.1016/j.talanta.2018.02.088
25. X. Zhang, "Gold nanoparticles: Recent advances in the biomedical applications," Cell Biochem. Biophys. **72** (3), 771–775 (2015). https://doi.org/10.1007/s12013-015-0529-4
26. K. Maximova, A. Aristov, M. Sentis, and A. V. Kabashin, "Size-controllable synthesis of bare gold nanoparticles by femtosecond laser fragmentation in water," Nanotechnology, **26** (6), 065601 (2015). https://doi.org/10.1088/0957-4484/26/6/065601
27. V. I. Mazhukin, "Kinetics and dynamics of phase transformations in metals under action of ultra-short high-power laser pulses," in *Laser Pulses—Theory*, *Technology*, *and Applications*, Ed. by I. Peshko (InTech, Rijeka, Croatia, 2012), Chapter 8, pp. 219–276. https://doi.org/10.5772/50731.
28. N. W. Ashcroft and N. D. Mermin, *Solid State Physics* (Harcourt/Saunders College Publishing, Fort Worth, TX, 1976; Mir, Moscow, 1979).
29. Z. Tong, S. Li, X. Ruan, and H. Bao, "Comprehensive first-principles analysis of phonon thermal conductivity and electron–phonon coupling in different metals," Phys. Rev. B **100** (14), 144306 (2019). https://doi.org/10.1103/PhysRevB.100.144306
30. A. Principi, M. Carrega, M. B. Lundeberg, A. Woessner, F. H. L. Koppens, G. Vignale, and M. Polini, "Plasmon losses due to electron–phonon scattering: The case of graphene encapsulated in hexagonal boron nitride," Phys. Rev. B **90** (16), 165408 (2014). https://doi.org/10.1103/PhysrRevB.90.165408
31. P. B. Allen, "Theory of thermal relaxation of electrons in metals," Phys. Rev. Lett. **59** (13), 1460–1463 (1987). https://doi.org/10.1103/PhysRevLett.59.1460
32. M. Bernardi, J. Mustafa, J. B. Neaton, and S. G. Louie, "Theory and computation of hot carriers generated by surface plasmon polaritons in noble metals," Nat. Commun. **6**, 7044 (2015). https://doi.org/10.1038/ncomms8044
33. V. I. Mazhukin, M. G. Lobok, and B. N. Chichkov, "Modeling of fast phase transitions dynamics in metal target irradiated by pico- and femtosecond pulsed laser," Appl. Surf. Sci. **255** (10), 5112–5115 (2009). https://doi.org/10.1016/j.apsusc.2008.08.014
34. M. V. Shugaev, M. He, Y. Levy, A. Mazzi, A. Miotello, N. M. Bulgakova, and L. V. Zhigilei, "Laser-induced thermal processes: Heat transfer, generation of stresses, melting and solidification, vaporization, and phase explosion," in *Handbook of Laser Micro- and Nano-Engineering*, Ed. by K. Sugioka (Springer, Cham., 2021), pp. 1–81. https://doi.org/10.1007/978-3-319-69537-2_11-1
35. R. Venkatasubramanian, E. Siivola, T. Colpitts, and B. O'Quinn, "Thin-film thermoelectric devices with high room-temperature figures of merit," Nature **413**, 597–602 (2001). https://doi.org/10.1038/35098012
36. L. Zhang, J.-T. Lü, J.-S. Wang, and B. Li, "Thermal transport across metal–insulator interface via electron–phonon interaction," J. Phys.: Condens. Matter, **25** (44), 445801, 1–8 (2013). https://doi.org/10.1088/0953-8984/25/44/445801
37. N. Singh, "Relaxation between electrons and surface phonons of a homogeneously photoexcited metal film," Pramana **63** (5), 1083–1087 (2004). https://doi.org/10.1007/bf02704347
38. A. J. Minnich, J. A. Johnson, A. J. Schmidt, K. Esfarjani, M. S. Dresselhaus, K. A. Nelson, and G. Chen, "Thermal conductivity spectroscopy technique to measure phonon mean free paths," Phys. Rev. Lett. **107** (9), 09591, 1–4 (2011). https://doi.org/10.1103/PhysRevLett.107.095901
39. K. T. Regner, D. P. Sellan, Z. Su, C. H. Amon, A. J. H. McGaughey, and J. A. Malen, "Broadband phonon mean free path contributions to thermal conductivity measured using frequency domain thermoreflectance," Nat. Commun. **4** (1), 1640, 1–7 (2013). https://doi.org/10.1038/ncomms2630
40. R. B. Wilson, J. P. Feser, G. T. Hohensee, and D. G. Cahill, "Two-channel model for nonequilibrium thermal transport in pump-probe experiments," Phys. Rev. B **88** (14), 144305, 1–11 (2013). https://doi.org/10.1103/physrevb.88.144305
41. K. T. Regner, J. P. Freedman, and J. A. Malen, "Advances in studying phonon mean free path dependent contributions to thermal conductivity," Nanoscale Microscale Thermophys. Eng. **19** (3), 183–205 (2015). https://doi.org/10.1080/15567265.2015.1045640

42. V. V. Zhakhovskii, N. A. Inogamov, Yu. V. Petrov, S. I. Ashitkov, and K. Nishihara, "Molecular dynamics simulation of femtosecond ablation and spallation with different interatomic potentials," Appl. Surf. Sci. **255** (24), 9592–9596 (2009).
https://doi.org/10.1016/j.apsusc.2009.04.082

43. L. Verlet, "Computer "Experiments" on classical fluids. I. Thermodynamical Properties of Lennard-Jones molecules," Phys. Rev. **159** (1), 98–103 (1967).
https://doi.org/10.1103/PhysRev.159.98

44. S. Plimpton, "Fast parallel algorithms for short-range molecular dynamics," J. Comput. Phys. **117** (1), 1–19 (1995).
https://doi.org/10.1006/jcph.1995.1039

45. H. J. C. Berendsen, J. P. M Postma, W. F. van Gunsteren, A. DiNola, and J. R. Haak, "Molecular dynamics with coupling to an external bath," J. Chem. Phys. **81** (8), 3684–3690 (1984).
https://doi.org/10.1063/1.448118

46. *Physical Quantities. A Handbook*, Ed. by I. S. Grigoriev and E. Z. Melikhov (Energoatomizdat, Moscow, 1991) [in Russian].

47. V. E. Zinoviev, *Thermophysical Properties of Metals at High Temperatures* (Metallurgiya, Moscow, 1989) [in Russian].

48. G. Wilde, C. Mitsch, G. P. Görler, and R. Willnecker, "Specific heat and related thermodynamic functions of undercooled Cu-Ni and Au melts," J. Non-Cryst. Solids **205–207** (Part 1), 425–429 (1996).
https://doi.org/10.1016/S0022-3093(96)00451-6

49. E. Kaschnitz, G. Nussbaumer, G. Pottlacher, and H. Jäger, "Microsecond-resolution measurements of the thermophysical properties of liquid gold," Int. J. Thermophys. **14** (2), 251–257 (1993).
https://doi.org/10.1007/BF00507812

50. J. W. Arblaster, "Thermodynamic properties of gold," J. Phase Equilib. Diffus. **37** (2), 229–245 (2016).
https://doi.org/10.1007/s11669-016-0449-z

51. J. W. Tester, R. C. Feber, and C. C. Herrick, "Calorimetric study of liquid gold," J. Chem. Eng. Data **13** (3), 419–421 (1968).
https://doi.org/10.1021/je60038a035

52. A. T. Dinsdale, "SGTE data for pure elements," Calphad **15** (4), 317–425 (1991).
https://doi.org/10.1016/0364-5916(91)90030-N

53. W. J. Evans and P. Keblinski, "Thermal conductivity of carbon nanotube cross-bar structures," Nanotechnology **21** (47), 475704 (2010).
https://doi.org/10.1088/0957-4484/21/47/475704

54. F. Müller-Plathe, "A simple nonequilibrium molecular dynamics method for calculating the thermal conductivity," J. Chem. Phys. **106** (14), 6082–6085 (1997).
https://doi.org/10.1063/ 1.473271

55. S. Ju and X. Liang, "Thermal conductivity of nanocrystalline silicon by direct molecular dynamics simulation," J. Appl. Phys. **112**, 064305 (2012).
https://doi.org/10.1063/1.4752266

56. O. N. Koroleva, M. M. Demin, A. V. Mazhukin, and V. I. Mazhukin, "Modeling of electronic and phonon thermal conductivity of silicon in a wide temperature range," J. Phys.: Conf. Ser. **1787**, 012026 (2021).
https://doi.org/10.1088/1742-6596/1787/1/012026

57. M. M. Demin, O. N. Koroleva, A. A. Aleksashkina, and V. I. Mazhukin, "Molecular-dynamic modeling of thermophysical properties of the phonon subsystem of copper in wide temperature range," Math. Montis. **47**, 137–151 (2020).
https://doi.org/10.20948/mathmontis-2020-47-12

58. D. P. Sellan, E. S. Landry, J. E. Turney, A. J. H. McGaughey, and C. H. Amon, "Size effects in molecular dynamics thermal conductivity predictions," Phys. Rev. B **81** (21), 214305 (2010).
https://doi.org/10.1103/PhysRevB.81.214305

59. P. K. Schelling, S. R. Phillpot, and P. Keblinski, "Comparison of atomic-level simulation methods for computing thermal conductivity," Phys. Rev. B **65** (14), 144306 (2002).
https://doi.org/10.1103/PhysRevB.65.144306

60. L. Hu, W. J. Evans, and P. Keblinski, "One-dimensional phonon effects in direct molecular dynamics method for thermal conductivity determination," J. Appl. Phys. **110** (11), 113511 (2011).
https://doi.org/10.1063/1.3660234

61. A. Jain and A. J. H. McGaughey, "Thermal transport by phonons and electrons in aluminum, silver, and gold from first principles," Phys. Rev. B **93** (8), 081206(R) (2016).
https://doi.org/10.1103/PhysRevB.93.081206

62. Y. Wang, Z. Lu, and X. Ruan, "First principles calculation of lattice thermal conductivity of metals considering phonon-phonon and phonon-electron scattering," J. Appl. Phys. **119** (22), 225109 (2016). https://doi.org/10.1063/1.4953366
63. N. Stojanovic, D. H. S. Maithripala, J. M. Berg, and M. Holtz, "Thermal conductivity in metallic nanostructures at high temperature: Electrons, phonons, and the Wiedemann-Franz law," Phys. Rev. B **82** (7), 075418 (2010). https://doi.org/10.1103/PhysRevB.82.075418
64. V. I. Mazhukin, A. V. Shapranov, and O. N. Koroleva, "Atomistic modeling of crystal-melt interface mobility of fcc (Al, Cu) and bcc (Fe) metals in strong superheating/undercooling states," Math. Montis. **48**, 70–85 (2020). https://doi.org/10.20948/mathmontis-2020-48-7
65. V. I. Mazhukin, A. V. Shapranov, and V. E. Perezhigin, "Mathematical modeling of thermophysical properties, metal heating and melting processes by the molecular dynamics method," Math. Montis. **24**, 47–65 (2012) [in Russian].
66. K. Lu and Y. Li, "Homogeneous nucleation catastrophe as a kinetic stability limit for superheated crystal," Phys. Rev. Lett. **80** (20), 4474–4477 (1998). https://doi.org/10.1103/physrevlett.80.4474